ACCSCIENCE PUBLISHING
An International Journal of Optimization and Control: Theories & Applications
ISSN: 2146-0957 eISSN: 2146-5703
Vol.x, No.x, pp.xx-xx (2026)
https://doi.org/10.36922/IJOCTA026390293
IJOCTA
RESEARCH ARTICLE

An efficient localized RBF-HFD approach for time-fractional convection–diffusion–reaction optimal control problems

Omid Nikan*

School of Mathematics and Computer Science, Iran University of Science and Technology, Narmak, Tehran, Iran
nikan@iust.ac.ir

ARTICLE INFO

Article history:
Received: September 25, 2026
Revised: Ocotber 24, 2026
Accepted: November 16, 2026
Published Online: November 17, 2026

Keywords:
TFCDR-OCPs
Shifted Grünwald formula
RBF-HFD method
Meshless collocation
Stability and convergence

AMS Classification 2020:
35R11; 49J20; 65M06; 65M12

ABSTRACT

This paper presents an efficient localized meshless collocation method for solving time-fractional convection–diffusion–reaction optimal control problems (TFCDR-OCPs). The proposed method consists of two main components. First, the time-fractional derivative is discretized using a shifted Grünwald scheme. The spatial derivatives appearing in the state and adjoint equations are then approximated by a localized radial basis function Hermite finite-difference (RBF-HFD) method. In this approach, the spatial differential operators are approximated locally over small overlapping neighborhoods, which avoids the need to construct and solve large global interpolation systems. The stability and convergence of the resulting numerical scheme are also investigated theoretically. Finally, three numerical examples are presented to evaluate the accuracy and computational performance of the proposed method.

CC BY

1. Introduction

Optimal control problems (OCPs) involving fractional differential equations have received increasing attention in recent years because of their importance in many scientific and engineering applications.[1–4] Convection–diffusion optimal control problems also appear in several practical fields, such as air pollution control,[5] dynamical systems[6] and wastewater treatment processes.[7] For example, in air pollution problems, the aim is to control pollutant sources so that the concentration of pollutants remains close to a desired level while the control cost is kept as low as possible. In this setting, the source term is regarded as the control variable, whereas the pollutant concentration represents the state variable. Partial Differential Equation (PDE)-constrained optimal control problems have been widely studied because of their practical importance and the computational challenges involved in their numerical solution. Two main approaches are commonly used: the optimize-then-discretize (OD) approach[8] and the discretize-then-optimize (DO) approach.[9–11] In the OD approach, the optimality conditions are first derived at the continuous level. The resulting state, adjoint, and control equations are then discretized by numerical techniques such as finite-difference methods[12] or finite-element methods.[13] The resulting algebraic system can then be solved by suitable iterative techniques.[14,15] In the DO approach, the governing PDEs are first discretized, which converts the original problem into a finite-dimensional optimization problem. This discrete problem is then solved using appropriate optimization algorithms.[16,17] Although this approach is often easier to implement, the construction of the corresponding KKT system may become complicated in the presence of general constraints, and some discretization schemes may lead to nonsymmetric algebraic systems.[9] Several numerical methods have also been developed for fractional OCPs. Tajadodi *et al.*[18] used Genocchi polynomials and an operational-matrix technique

*Corresponding Author

to obtain numerical solutions for a class of OCPs. Baleanu *et al.*[19] proposed a finite-difference method for delay-dependent fractional OCPs and analyzed the accuracy and convergence of the proposed scheme. Youssri and Abd-Elhameed[20] introduced a spectral tau method based on Jacobi polynomials for solving fractional OCPs. Hassani *et al.*[21] applied generalized shifted Chebyshev polynomials to fractional OCPs. They later developed a hybrid approach for two-dimensional nonlinear variable-order fractional optimal control problems.[22] Hassani *et al.*[23] employed generalized Bernoulli polynomials and operational matrices to solve nonlinear fractional OCPs.

Let Ω be a bounded region in $\mathbb{R}^d$, with $d \in \{1, 2, 3\}$, and let $\partial\Omega$ denote its boundary. For a fixed terminal time $T > 0$, the space–time cylinder is defined as $Q = \Omega \times (0, T]$, with the corresponding lateral boundary given by $\Sigma = \partial\Omega \times (0, T]$. In this work, we focus on the numerical solution of the following time-fractional convection–diffusion–reaction optimal control problem (TFCDR-OCP):

$$\begin{aligned}\min_{u\in U_{ad}} J(y,u) := \frac{\lambda}{2}\left\|u(\mathbf{x},t)\right\|^2_{L_2(Q)} \\ + \frac{1}{2}\left\|y(\mathbf{x},t) - y_d(\mathbf{x},t)\right\|^2_{L_2(Q)}.\end{aligned} \tag{1}$$

subject to the state system

$$\begin{cases}\dfrac{\partial^{\beta} y(\mathbf{x},t)}{\partial t^{\beta}} - \Delta y(\mathbf{x},t) - \mathbf{v}(\mathbf{x})\cdot\nabla y(\mathbf{x},t) \\ + w(\mathbf{x})y(\mathbf{x},t) = u(\mathbf{x},t), (\mathbf{x},t)\in Q, \\ y(\mathbf{x},0) = y_0(\mathbf{x}), \mathbf{x}\in\Omega, \\ y(\mathbf{x},t) = g(\mathbf{x},t), (\mathbf{x},t)\in\Sigma.\end{cases} \tag{2}$$

In problem (1), the desired state is represented by $y_d(\mathbf{x}, t)$, whereas $u(\mathbf{x}, t)$ and $y(\mathbf{x}, t)$ stand for the control and state functions, respectively. The parameter $\lambda > 0$ is the regularization parameter. The admissible control set is defined by

$$U_{ad} = \{u \in L_2(\Omega) \mid u(\mathbf{x}) \in [a, b] \text{ for almost every } \mathbf{x} \in \Omega\}.$$

where

$$a, b \in \mathbb{R} \cup \{\pm\infty\}$$

are prescribed constant bounds. **Equation 2** represents a time-fractional convection–diffusion–reaction (TFCDR) equation of fractional order β. Here, $\mathbf{v}(\mathbf{x})$ denotes the convection velocity field, while $w(\mathbf{x})$ is the reaction coefficient. The functions $y_0(\mathbf{x})$ and $g(\mathbf{x}, t)$ are assumed to be continuous and represent the prescribed initial and Dirichlet boundary conditions, respectively. For $\beta \in (0, 1)$, the fractional derivative appearing in **Equation 2** is understood in the Caputo sense with respect to the time variable t, and is defined by

$$\frac{\partial^{\beta} y(\mathbf{x},t)}{\partial t^{\beta}} = \frac{1}{\Gamma(1-\beta)}\int_0^t \frac{\partial y(\mathbf{x},v)}{\partial v}\frac{\mathrm{d}v}{(t-v)^{\beta}}. \tag{3}$$

The TFCDR **Equation 2** models a broad class of chemical and industrial systems in which convection, diffusion, and reaction processes occur simultaneously.

1.1. Derivation of the optimality system

The Lagrangian formulation is employed to derive the optimality conditions associated with the TFCDR-OCP. Introducing p as the adjoint variable and enforcing the first-order stationarity conditions of the corresponding Lagrangian functional[24,25] leads to the optimality system, which is composed of the state equation,

$$\begin{cases} wy^* - \mathbf{v}\cdot\nabla y^* - \Delta y^* + \partial_t^{\beta} y^* = u^*, \\ (\mathbf{x},t)\in Q, \\ y^*(\mathbf{x},0) = y_0(\mathbf{x}), \mathbf{x}\in\Omega, \\ y^* = g, (\mathbf{x},t)\in\Sigma, \end{cases} \tag{4}$$

while the corresponding adjoint equation is given by

$$\begin{cases} wp^* - \Delta p^* - \mathbf{v}\cdot\nabla p^* - \partial_t^{\beta} p^* = y^* - y_d, \\ (\mathbf{x},t)\in Q, \\ p^*(\mathbf{x},T) = 0, \mathbf{x}\in\Omega, \\ p^* = g, (\mathbf{x},t)\in\Sigma. \end{cases} \tag{5}$$

The gradient condition follows by differentiating with respect to the control variable u and is expressed as:

$$p^* + \lambda u^* = 0. \tag{6}$$

Accordingly, the optimality system given by **Equations 4–6** can be recast in the following form:

$$\begin{cases} \partial_t^{\beta} y^* + wy^* - \mathbf{v}\cdot\nabla y^* - \Delta y^* = -\dfrac{1}{\lambda}p^*, \\ (\mathbf{x},t)\in Q, \\ -\partial_t^{\beta} p^* + wp^* - \mathbf{v}\cdot\nabla p^* - \Delta p^* \\ = y^* - y_d, (\mathbf{x},t)\in Q. \end{cases} \tag{7}$$

supplemented by the following initial and terminal conditions:

$$\begin{cases} p^*(\mathbf{x},T) = 0, & \mathbf{x}\in\Omega, \\ y^*(\mathbf{x},0) = y_0(\mathbf{x}), & \mathbf{x}\in\Omega. \end{cases} \tag{8}$$

The corresponding Dirichlet boundary conditions are given by

$$\begin{cases} y^*(\mathbf{x},t) = g(\mathbf{x},t), & \text{over } \Sigma, \\ p^*(\mathbf{x},t) = g(\mathbf{x},t), & \text{over } \Sigma. \end{cases} \tag{9}$$

Darehmiraki and Rezazadeh[26] investigated a TFCDR-OCP, derived the necessary optimality conditions through a Lagrangian formulation, and solved the resulting system using a rational barycentric collocation (RBC) method. Mahmoudi *et al.*[27] investigated a TFCDR-OCP and developed a local compact integrated radial basis function (CIRBF) method for its numerical solution.

In this paper, we introduce a localized numerical method for solving TFCDR-OCPs. The proposed approach combines a shifted Grünwald formula for the approximation of the time-fractional derivative with a localized RBF Hermite finite-difference (RBF-HFD) scheme for the spatial discretization. Owing to its local structure, the method avoids the construction of large global RBF systems and provides an efficient treatment of both the adjoint and state equations. The stability and convergence properties of the resulting scheme are established theoretically. In addition, three numerical examples are considered to assess its accuracy and computational performance.

The paper is organized as follows. Section 2 describes the temporal discretization of the optimality system based on the shifted Grünwald formula and provides the corresponding stability and convergence analysis. Section 3 describes the local RBF-HFD spatial discretization and the construction of the local approximation operators. Section 4 reports three numerical examples that illustrate the accuracy and computational performance of the proposed strategy. Finally, Section 5 highlights the main findings and concludes the paper.

2. Temporal discretization

This section describes the temporal discretization of the optimality system. The temporal interval $[0,T]$ is partitioned into N_t uniform subintervals with time-step size $\delta t = T/N_t$, where T denotes the final time. The corresponding discrete time levels are defined by $t_m = m\delta t,\ m = 0,1,\ldots,N_t$. For the spatial discretization, we consider the set $\Omega_h = \{(x_i,y_j) : 0 \le i,j \le N,\ x_i = ih,\ y_j = jh\}$, where N denotes the number of spatial subdivisions and h is the associated spatial step size. To derive a semi-discrete form of **Equation 7**, the time-fractional derivative is numerically evaluated by means of the shifted Grünwald formula.

Lemma 1. Assume that $y(t) \in C^2[0,+\infty)$, $\frac{d^3y(t)}{dt^3} \in L^1[0,+\infty)$, and that $y''(0) = y'(0) = 0$. For $\beta \in (0,1)$ and any integer k, the Caputo derivative of fractional order β evaluated at $t_m + \left(k - \frac{\beta}{2}\right)\delta t$ can be approximated with second-order accuracy by the shifted Grünwald formula:

$$
\begin{aligned}
&{}_0^C D_t^\beta y\left[t_m + \left(k - \frac{\beta}{2}\right)\delta t\right] = \frac{1}{\delta t^\beta}\sum_{n=0}^{m}\omega_n \\
&\left(y^{m+k-n} - y^0\right) + O(\delta t^2).
\end{aligned}
\tag{10}
$$

By setting $k = 0$, the above formula reduces to the following special case:

$$
\begin{aligned}
&{}_0^C D_t^\beta y\left(t_m - \frac{\beta}{2}\delta t\right) = \frac{1}{\delta t^\beta}\sum_{n=0}^{m}\omega_n \\
&\left(y^{m-n} - y^0\right) + O(\delta t^2).
\end{aligned}
\tag{11}
$$

The coefficients ω_n are obtained recursively from

$$
(1-z)^\beta = \sum_{n=0}^{\infty}\omega_n z^n, \tag{12}
$$

and satisfy

$$
\omega_0 = 1, \qquad \omega_n = \left(1 - \frac{1+\beta}{n}\right)\omega_{n-1}, \qquad n \ge 1,
$$

together with

$$
\omega_1 < \omega_2 < \cdots < \omega_m < \cdots < 0, \quad \sum_{n=0}^{\infty}|\omega_n| = 1.
$$

Suppose that

$$
y(x_i,y_j,t_m) = y_{ij}^m, \quad 1 \le i,j \le N, m = 0,\ldots,N_t.
$$

By evaluating **Equation 7** at the point $(x_i,y_j,t_{m-\beta/2})$ and invoking Lemma 1, the following relation is obtained:

$$
\begin{cases}
\dfrac{1}{\delta t^\beta}\displaystyle\sum_{n=0}^{m}\omega_n\left(y_{ij}^{m-n} - y_{ij}^0\right) - \Delta y_{ij}^{m-\frac{\beta}{2}} \\
- \mathbf{v}_{ij}\cdot\nabla y_{ij}^{m-\frac{\beta}{2}} + w y_{ij}^{m-\frac{\beta}{2}} \\
= -\dfrac{1}{\lambda}p_{ij}^{m-\frac{\beta}{2}} + O(\delta t^2), \\
-\dfrac{1}{\delta t^\beta}\displaystyle\sum_{n=0}^{m}\omega_n\left(p_{ij}^{m-n} - p_{ij}^0\right) - \Delta p_{ij}^{m-\frac{\beta}{2}} \\
- \mathbf{v}_{ij}\cdot\nabla p_{ij}^{m-\frac{\beta}{2}} + w p_{ij}^{m-\frac{\beta}{2}} \\
= y_{ij}^{m-\frac{\beta}{2}} - y_{d,ij}^{m-\frac{\beta}{2}} + O(\delta t^2).
\end{cases}
\tag{13}
$$

By applying the weighted approximation,

$$
\Delta y_{ij}^{m-\frac{\beta}{2}} = \left(1 - \frac{\beta}{2}\right)\Delta y_{ij}^m + \frac{\beta}{2}\Delta y_{ij}^{m-1}, \tag{14}
$$

and neglecting the truncation errors, **Equation 13** can be rewritten as

$$
\begin{cases}
\displaystyle\sum_{n=0}^{m}\omega_n\left(y_{ij}^{m-n} - y_{ij}^0\right) - \delta t^\beta\left(1 - \frac{\beta}{2}\right) \\
\mathcal{L}_h y_{ij}^m - \delta t^\beta\dfrac{\beta}{2}\mathcal{L}_h y_{ij}^{m-1}
\end{cases}
\tag{15}
$$

$$\begin{cases} = -\dfrac{\delta t^{\beta}}{\lambda}\left[\left(1-\dfrac{\beta}{2}\right)p_{ij}^{m}+\dfrac{\beta}{2}p_{ij}^{m-1}\right], \\ -\displaystyle\sum_{n=0}^{m}\omega_n\left(p_{ij}^{m-n}-p_{ij}^{0}\right)-\delta t^{\beta}\left(1-\dfrac{\beta}{2}\right) \\ \mathcal{L}_h p_{ij}^{m}-\delta t^{\beta}\dfrac{\beta}{2}\mathcal{L}_h p_{ij}^{m-1} \\ = \delta t^{\beta}[\left(1-\dfrac{\beta}{2}\right)\left(y_{ij}^{m}-y_{d,ij}^{m}\right) \\ +\dfrac{\beta}{2}\left(y_{ij}^{m-1}-y_{d,ij}^{m-1}\right)], \end{cases}$$

where, for notational convenience, the discrete spatial operator is defined as $\mathcal{L}_h = D_{2x}+D_{2y}+\mathbf{v}\cdot(D_{1x}+D_{1y})-w$. Taking into account that $\omega_0 = 1$, **Equation 15** can be expressed as

$$\begin{cases} \left[1-\delta t^{\beta}\left(1-\dfrac{\beta}{2}\right)\mathcal{L}_h\right]y_{ij}^{m} \\ +\dfrac{\delta t^{\beta}}{\lambda}\left(1-\dfrac{\beta}{2}\right)p_{ij}^{m} \\ \quad =-\displaystyle\sum_{n=1}^{m}\omega_n\left(y_{ij}^{m-n}-y_{ij}^{0}\right) \\ +\delta t^{\beta}\dfrac{\beta}{2}\mathcal{L}_h y_{ij}^{m-1}-\dfrac{\delta t^{\beta}}{\lambda}\dfrac{\beta}{2}p_{ij}^{m-1}+y_{ij}^{0}, \\ \left[1+\delta t^{\beta}\left(1-\dfrac{\beta}{2}\right)\mathcal{L}_h\right]p_{ij}^{m} \\ +\delta t^{\beta}\left(1-\dfrac{\beta}{2}\right)\left(y_{ij}^{m}-y_{d,ij}^{m}\right) \\ =-\displaystyle\sum_{n=1}^{m}\omega_n\left(p_{ij}^{m-n}-p_{ij}^{0}\right)-\delta t^{\beta}\dfrac{\beta}{2}\mathcal{L}_h p_{ij}^{m-1} \\ -\delta t^{\beta}\dfrac{\beta}{2}\left(y_{ij}^{m-1}-y_{d,ij}^{m-1}\right)-p_{ij}^{0}. \end{cases} \tag{16}$$

2.1. Stability and error analysis

Following the approach presented in,[27] the convergence and stability of the semi-discrete scheme (16) are investigated under the initial condition $y(\mathbf{x},0) = y_0(\mathbf{x})$ and the homogeneous Dirichlet boundary conditions $y^m|_{\partial\Omega} = 0$ for $0 \le m \le N_t$. The analysis is based on Lemma 1 and an energy-based argument. To this end, the space $L_2(\Omega)$ is considered, with the inner product and associated norm defined as

$$\langle v, y\rangle = \int_{\Omega} v(\mathbf{x})\, y(\mathbf{x})\, \mathrm{d}\mathbf{x}, \tag{17}$$

with the associated norm

$$\|y\|_2 = \left(\int_{\Omega} |y(\mathbf{x})|^2\, \mathrm{d}\mathbf{x}\right)^{1/2}. \tag{18}$$

Proposition 1. Let $(y^m, p^m) \in H_0^2(\Omega)\times H_0^2(\Omega)$, $0 \le m \le N_t$, denote the approximate solution pair obtained from the semi-discrete scheme (16), with the initial pair (y^0, p^0) assumed to be known. Assume that

$$p_{ij}^{m} \le y_{ij}^{m}, \qquad 1 \le i,j \le N, \qquad 1 \le m \le N_t.$$

Then, we have

$$\begin{cases} \|y^m\|_2^2 + c_1\left(\|\nabla y^m\|_2^2+\|p^m\|_2^2\right) \\ \le K_1\left(\|y^0\|_2^2+\|\nabla y^0\|_2^2+\|p^0\|_2^2\right), \\ \|p^m\|_2^2 \le K_2(\|p^0\|_2^2+\|\nabla p^0\|_2^2+\|y^0\|_2^2 \\ +\|\nabla y^0\|_2^2+\displaystyle\sum_{n=0}^{M}\|y_d^n\|_2^2). \end{cases} \tag{19}$$

Otherwise,

$$\begin{cases} \|y^m\|_2^2 + c_1\|\nabla y^m\|_2^2 \\ \le K_1\left(\|y^0\|_2^2+\|\nabla y^0\|_2^2+\|p^0\|_2^2\right), \\ \|p^m\|_2^2 + c_2\|y^m\|_2^2 \le K_2(\|p^0\|_2^2+\|\nabla p^0\|_2^2 \\ +\|y^0\|_2^2+\|\nabla y^0\|_2^2+\displaystyle\sum_{n=0}^{M}\|y_d^n\|_2^2). \end{cases} \tag{20}$$

Proof. The proof proceeds by mathematical induction. For the base case $m = 1$, **Equation 16** reduces to

$$\begin{cases} y^1 - c_1\Delta y^1 - c_1\mathbf{v}\cdot\nabla y^1 + c_1 w y^1 + \dfrac{c_1}{\lambda}p^1 \\ = c_2\Delta y^0 + c_2\mathbf{v}\cdot\nabla y^0 - c_2 w y^0 - \dfrac{c_2}{\lambda}p^0 + y^0, \\ p^1 + c_1\Delta p^1 + c_1\mathbf{v}\cdot\nabla p^1 - c_1 w p^1 + c_1(y^1 - y_d^1) \\ = -c_2\Delta p^0 - c_2\mathbf{v}\cdot\nabla p^0 + c_2 w p^0 \\ - c_2(y^0 - y_d^0) - p^0, \end{cases} \tag{21}$$

where $c_1 = \delta t^{\beta}\left(1-\frac{\beta}{2}\right)$ and $c_2 = \delta t^{\beta}\frac{\beta}{2}$. Multiplying the two relations in **Equaiont 21** by y^1 and p^1, respectively, followed by integration over Ω, leads to

$$\begin{cases} (y^1,y^1) - c_1 d_1(\Delta y^1, y^1) \\ - c_1 d_1(\mathbf{v}\cdot\nabla y^1, y^1) + \dfrac{c_1 d_1}{\lambda}(p^1, y^1) \\ = c_2 d_1(\Delta y^0, y^1) + c_2 d_1(\mathbf{v}\cdot\nabla y^0, y^1) \\ + (1-c_2 w) d_1(y^0, y^1) - \dfrac{c_2 d_1}{\lambda}(p^0, y^1), \\ (p^1,p^1) + c_1 d_2(\Delta p^1, p^1) \\ + c_1 d_2(\mathbf{v}\cdot\nabla p^1, p^1) + c_1 d_2(y^1 - y_d^1, p^1) \\ = -c_2 d_2(\Delta p^0, p^1) - c_2 d_2(\mathbf{v}\cdot\nabla p^0, p^1) \\ - (1-c_2 w) d_2(p^0, p^1) \\ - c_2 d_2(y^0 - y_d^0, p^1), \end{cases} \tag{22}$$

in which $d_1 = \frac{1}{1+c_1 w}$ and $d_2 = \frac{1}{1-c_1 w}$. By using the following Green's formula:

$$\int_{\Omega}\nabla v\cdot\nabla w\, \mathrm{d}\mathbf{x} = \int_{\partial\Omega} v\frac{\partial w}{\partial n}\, \mathrm{d}s - \int_{\Omega} v\Delta w\, \mathrm{d}\mathbf{x},$$

where

$$\frac{\partial w}{\partial n} = \frac{\partial w}{\partial x}n_1 + \frac{\partial w}{\partial y}n_2$$

represents differentiation in the outward normal direction on $\partial\Omega$, we then introduce

$$\alpha_1 = c_1 d_1, \quad \alpha_2 = c_2 d_1, \quad \alpha_3 = (1 - c_2 w) d_1,$$

and

$$\beta_1 = c_1 d_2, \quad \beta_2 = c_2 d_2, \quad \beta_3 = (1 - c_2 w) d_2.$$

Then, we have

$$\begin{cases} \|y^1\|_2^2 + \alpha_1 \|\nabla y^1\|_2^2 + \dfrac{\alpha_1}{\lambda}(p^1, y^1) \\ = -\alpha_2(\nabla y^0, \nabla y^1) + \alpha_2(\mathbf{v} \cdot \nabla y^0, y^1) \\ + \alpha_3(y^0, y^1) - \dfrac{\alpha_2}{\lambda}(p^0, y^1), \\ \|p^1\|_2^2 - \beta_1 \|\nabla p^1\|_2^2 + \beta_1(y^1 - y_d^1, p^1) \\ = \beta_2(\nabla p^0, \nabla p^1) - \beta_2(\mathbf{v} \cdot \nabla p^0, p^1) \\ - \beta_3(p^0, p^1) - \beta_2(y^0 - y_d^0, p^1). \end{cases} \tag{23}$$

At this stage, we use the property $y^1, p^1 \in H_0^2(\Omega)$, which immediately implies that

$$(\mathbf{v} \cdot \nabla y^1, y^1) = 0 = (\mathbf{v} \cdot \nabla p^1, p^1). \tag{24}$$

Combining Young's inequality with the condition $p_{ij}^m \leq y_{ij}^m$ and choosing the parameter $\lambda = 2$, we further assume that

$$\|\nabla p^m\|_2 \leq \|p^m\|_2, \qquad 1 \leq m \leq N_t.$$

We conclude:

$$\begin{cases} \|y^1\|_2^2 + \alpha_1 \left(\|\nabla y^1\|_2^2 + \|p^1\|_2^2 \right) \\ \leq \left(\dfrac{\alpha_2^2}{\alpha_1} + 3\alpha_2 v \right) \|\nabla y^0\|_2^2 \\ + 3\alpha_3 \|y^0\|_2^2 + \dfrac{3\alpha_2}{2} \|p^0\|_2^2, \\ \|p^1\|_2^2 \leq (20\beta_2 v + 2\beta_2) \|\nabla p^0\|_2^2 \\ + 20\beta_3 \|p^0\|_2^2 \\ + 20\beta_2 \|y^0\|_2^2 + 20\beta_1 \|y_d^1\|_2^2 + 20\beta_2 \|y_d^0\|_2^2. \end{cases} \tag{25}$$

Since $\|\nabla y^0\|_2^2$ is nonnegative, it follows that

$$\begin{cases} \|y^1\|_2^2 + \alpha_1 \left(\|\nabla y^1\|_2^2 + \|p^1\|_2^2 \right) \\ \leq K_1 \left(\|\nabla y^0\|_2^2 + \|y^0\|_2^2 + \|p^0\|_2^2 \right), \\ \|p^1\|_2^2 \leq K_2 (\|p^0\|_2^2 + \|\nabla p^0\|_2^2 + \|y^0\|_2^2 \\ + \|\nabla y^0\|_2^2 + \sum_{n=0}^{M} \|y_d^n\|_2^2). \end{cases} \tag{26}$$

Assume now that the assertion holds for all $j = 1, \ldots, m-1$. Then, it follows that

$$\begin{cases} \|y^j\|_2^2 + c_1 \left(\|\nabla y^j\|_2^2 + \|p^j\|_2^2 \right) \\ \leq K_1 \left(\|y^0\|_2^2 + \|\nabla y^0\|_2^2 + \|p^0\|_2^2 \right), \\ \|p^j\|_2^2 \leq K_2 (\|p^0\|_2^2 + \|\nabla p^0\|_2^2 + \|y^0\|_2^2 \\ + \|\nabla y^0\|_2^2 + \sum_{n=0}^{M} \|y_d^n\|_2^2). \end{cases} \tag{27}$$

Taking the inner products of the two equations in **Equation 16** with y^m and p^m, respectively, over Ω, we obtain

$$\begin{cases} (y^m, y^m) + \dfrac{\alpha_1}{\lambda}(y^m, p^m) - \alpha_1(y^m, \mathbf{v} \cdot \nabla y^m) \\ - \alpha_1(y^m, \Delta y^m) \\ = d_1(y^m, y^0) - \dfrac{\alpha_2}{\lambda}(y^m, p^{m-1}) \\ - \alpha_2 w(y^m, y^{m-1}) \\ + \alpha_2(y^m, \mathbf{v} \cdot \nabla y^{m-1}) + \alpha_2(y^m, \Delta y^{m-1}) \\ - d_1 \sum_{n=1}^{m} \omega_n \left(y^m, y^{m-n} - y^0 \right), \\ (p^m, p^m) + \beta_1(p^m, y^m - y_d^m) \\ + \beta_1(p^m, \mathbf{v} \cdot \nabla p^m) - \beta_1(p^m, \Delta p^m) \\ = -d_2(p^m, p^0) + \beta_2 w(p^m, p^{m-1}) \\ - \beta_2(p^m, y^{m-1} - y_d^{m-1}) \\ - \beta_2(p^m, \mathbf{v} \cdot \nabla p^{m-1}) - \beta_2(p^m, \Delta p^{m-1}) \\ - d_2 \sum_{n=1}^{m} \omega_n \left(p^m, p^{m-n} - p^0 \right). \end{cases} \tag{28}$$

Employing Green's identity together with the homogeneous boundary conditions yields

$$\begin{cases} (y^m, y^m) + \dfrac{\alpha_1}{\lambda}(y^m, p^m) \\ + \alpha_1(\nabla y^m, \nabla y^m) \\ = d_1(y^m, y^0) - \dfrac{\alpha_2}{\lambda}(y^m, p^{m-1}) \\ - \alpha_2 w(y^m, y^{m-1}) \\ + \alpha_2(y^m, \mathbf{v} \cdot \nabla y^{m-1}) \\ - \alpha_2(\nabla y^m, \nabla y^{m-1}) \\ - d_1 \sum_{n=1}^{m} \omega_n \left(y^m, y^{m-n} - y^0 \right), \\ (p^m, p^m) + \beta_1(p^m, y^m) \\ + \beta_1(\nabla p^m, \nabla p^m) \\ = \beta_1(p^m, y_d^m) - d_2(p^m, p^0) \\ + \beta_2 w(p^m, p^{m-1}) \\ - \beta_2(p^m, y^{m-1} - y_d^{m-1}) \\ - \beta_2(p^m, \mathbf{v} \cdot \nabla p^{m-1}) \\ + \beta_2(\nabla p^m, \nabla p^{m-1}) \\ - d_2 \sum_{n=1}^{m} \omega_n \left(p^m, p^{m-n} - p^0 \right). \end{cases} \tag{29}$$

By making use of Young's inequality, choosing $\lambda = 2$, and imposing the assumption

$$\|\nabla p^m\|_2 \leq \|p^m\|_2, \qquad 1 \leq m \leq N_t.$$

we obtain

$$\begin{cases} \|y^m\|_2^2 + \alpha_1 \left(\|\nabla y^m\|_2^2 + \|p^m\|_2^2\right) \\ \le 5d_1^2 \left(1 + \dfrac{d_1^2}{2}\right) \|y^0\|_2^2 \\ + 5\alpha_2 w \|y^{m-1}\|_2^2 \\ + \left(\dfrac{\alpha_2^2}{\alpha_1} + 5\alpha_2^2 v\right) \|\nabla y^{m-1}\|_2^2 \\ + 5\alpha_2^2 \|p^{m-1}\|_2^2 + \dfrac{5}{2} \displaystyle\sum_{n=1}^{m} |\omega_n| \, \|y^{m-n}\|_2^2, \\ \|p^m\|_2^2 \le (84 + 28d_2)\|p^0\|_2^2 \\ + (2\beta_2 + 28\beta_2 v)\|\nabla p^{m-1}\|_2^2 \\ + 28\beta_2 w \|p^{m-1}\|_2^2 + 28\beta_2 \|y^{m-1}\|_2^2 \\ + 84 d_2 \displaystyle\sum_{n=1}^{m} |\omega_n| \, \|p^{m-n}\|_2^2 \\ + 28\beta_1^2 \displaystyle\sum_{n=0}^{M} \|y_d^n\|_2^2. \end{cases} \tag{30}$$

Therefore, using **Equation 27** and

$$\|y^j\|_2^2 \le K_1 \left(\|y^0\|_2^2 + \|\nabla y^0\|_2^2 + \|p^0\|_2^2\right), \quad j = 1, \ldots, m-1,$$

we obtain **Equation 20**. The case $p_{ij}^m \ge y_{ij}^m$ is proved similarly, which completes the proof. □

Let y^m and p^m, $m = 0, 1, \ldots, N_t$, be the approximate solutions of **Equation 16** satisfying the initial and terminal conditions in **Equation 8**. The stability of the proposed scheme is established in the following theorem.

Theorem 1. Let $Y^m(\mathbf{x})$ and $P^m(\mathbf{x})$, $m = 0, 1, \ldots, N_t$, be the reference state and adjoint solutions at the discrete time levels, with $Y^m(\mathbf{x}), P^m(\mathbf{x}) \in H_0^1(\Omega)$. Then, provided that the assumptions of Proposition 1 are satisfied, the numerical scheme given by **Equation 16** is stable.

Proof. To measure the difference between the reference and numerical solutions, we set $\rho^m(\mathbf{x}) = Y^m(\mathbf{x}) - y^m(\mathbf{x})$ and $\zeta^m(\mathbf{x}) = P^m(\mathbf{x}) - p^m(\mathbf{x})$ for the state and adjoint errors, respectively. Applying Proposition 1 to the corresponding error equations gives

$$\begin{cases} \|\varepsilon^m\|_2^2 + c_1 \left(\|\nabla \rho^m\|_2^2 + \|\zeta^m\|_2^2\right) \\ \le K_1 \left(\|\rho^0\|_2^2 + \|\nabla \rho^0\|_2^2 + \|\zeta^0\|_2^2\right), \\ \|\zeta^m\|_2^2 \le K_2 (\|\zeta^0\|_2^2 + \|\nabla \zeta^0\|_2^2 + \|\rho^0\|_2^2 \\ + \|\nabla \rho^0\|_2^2 + \displaystyle\sum_{n=0}^{M} \|y_d^n\|_2^2). \end{cases} \tag{31}$$

Since

$$y^m|_{\partial\Omega} = 0, \qquad p^m|_{\partial\Omega} = 0,$$

Proposition 1 yields

$$\begin{cases} \|\rho^m\|_2^2 \le K_1 \left(\|\rho^0\|_2^2 + \|\nabla \rho^0\|_2^2 + \|\zeta^0\|_2^2\right), \\ \|\zeta^m\|_2^2 \le K_2 (\|\zeta^0\|_2^2 + \|\nabla \zeta^0\|_2^2 + \|\rho^0\|_2^2 \\ + \|\nabla \rho^0\|_2^2 + \displaystyle\sum_{n=0}^{M} \|y_d^n\|_2^2). \end{cases} \tag{32}$$

This completes the proof. □

3. Spatial discretization using the RBF–HFD method

Meshless methods avoid the need for a predefined mesh by approximating the solution over a set of scattered nodes distributed throughout the computational domain. This feature makes them particularly attractive for problems defined on complicated geometries. In comparison with traditional grid-based techniques, meshless collocation methods offer several advantages: they eliminate the cost of mesh generation, are well suited to complex-shaped domains, and can be extended more easily to multidimensional problems.[28] Among the most widely used meshless methods are RBF methods, which have received considerable attention in recent years. We first recall the standard RBF interpolation setting. Let $u : \Omega \to \mathbb{R}$ be a continuous function whose values are known at a set of distinct nodes

$$\mathbf{X} = \{\mathbf{x}_1, \mathbf{x}_2, \ldots, \mathbf{x}_M\}.$$

An RBF interpolant of u can be represented in the form

$$\mathbb{I}_{\mathbf{X},u}(\mathbf{x}) = \sum_{j=1}^{M} \lambda_j \phi\big(\|\mathbf{x} - \mathbf{x}_j\|\big) + \sum_{j=1}^{l} \nu_j p_j(\mathbf{x}), \tag{33}$$

where $\|\cdot\|$ denotes the Euclidean norm, ϕ is a radial basis function, and $\{p_j\}_{j=1}^{l}$ denotes a polynomial basis in the spatial variables. The unknown coefficients $\{\lambda_j\}_{j=1}^{M}$ and $\{\nu_j\}_{j=1}^{l}$ are determined by requiring the interpolant to reproduce the given nodal values,

$$\mathbb{I}_{\mathbf{X},u}(\mathbf{x}_j) = u(\mathbf{x}_j), \qquad j = 1, 2, \ldots, M, \tag{34}$$

together with the usual polynomial side conditions

$$\sum_{j=1}^{M} \lambda_j p_k(\mathbf{x}_j) = 0, \qquad k = 1, 2, \ldots, l. \tag{35}$$

These conditions lead to the block linear system

$$\begin{pmatrix} \mathbf{\Phi} & \mathbf{P} \\ \mathbf{P}^{\mathrm{T}} & \mathbf{0} \end{pmatrix} \begin{pmatrix} \boldsymbol{\lambda} \\ \boldsymbol{\nu} \end{pmatrix} = \begin{pmatrix} \mathbf{u} \\ \mathbf{0} \end{pmatrix}, \tag{36}$$

in which the entries of the RBF matrix are

$$\Phi_{i,j} = \phi\big(\|\mathbf{x}_i - \mathbf{x}_j\|\big), \qquad i, j = 1, 2, \ldots, M, \tag{37}$$

while the polynomial matrix is defined by

$$P_{i,j} = p_j(\mathbf{x}_i), i = 1, 2, \ldots, M, j = 1, 2, \ldots, l. \quad (38)$$

The coefficient and data vectors are written as

$$\boldsymbol{\lambda} = [\lambda_1, \lambda_2, \ldots, \lambda_M]^{\mathrm{T}}, \qquad \boldsymbol{\nu} = [\nu_1, \nu_2, \ldots, \nu_l]^{\mathrm{T}},$$

and

$$\mathbf{u} = [u(\mathbf{x}_1), u(\mathbf{x}_2), \ldots, u(\mathbf{x}_M)]^{\mathrm{T}}.$$

For distinct interpolation nodes, the block system (36) is nonsingular under the usual assumptions that ϕ is positive definite, or conditionally positive definite with a compatible polynomial space; see Wendland.[29] We now introduce the localized RBF–HFD formulation. The main idea is to enrich the standard local RBF finite-difference approximation by incorporating derivative information at a small number of neighboring nodes.[30,31] This provides additional local information without substantially increasing the number of function values involved in each stencil. For a center $\mathbf{x}_j$, let

$$\mathbf{X}_j = \left\{\mathbf{x}_1^{(j)}, \ldots, \mathbf{x}_m^{(j)}\right\} \subset \mathbf{X}$$

denote a local stencil consisting of $\mathbf{x}_j$ and its nearest neighbors, with $m \ll M$. In addition, consider a set of Hermite nodes

$$\widetilde{\mathbf{X}}_j = \left\{\widetilde{\mathbf{x}}_1^{(j)}, \ldots, \widetilde{\mathbf{x}}_q^{(j)}\right\} \subset \mathbf{X}.$$

For a linear differential operator $\mathcal{L}$, the RBF–HFD approximation at the stencil center is written as

$$\mathcal{L}u(\mathbf{x}_j) \approx \sum_{k=1}^{m} w_k^{(j)} u\big(\mathbf{x}_k^{(j)}\big) + \sum_{k=1}^{q} \widetilde{w}_k^{(j)} \mathcal{L}u\big(\widetilde{\mathbf{x}}_k^{(j)}\big). \quad (39)$$

Hence, the approximation makes use of both the function values on the local stencil and the values of the differential operator at selected Hermite nodes. The corresponding coefficients $w_k^{(j)}$ and $\widetilde{w}_k^{(j)}$ are chosen so that (39) is exact for the local approximation space generated by

$$\left\{\phi\big(\|\mathbf{x} - \mathbf{x}_i^{(j)}\|\big)\right\}_{i=1}^{m},$$

together with the derivative RBF approximations

$$\left\{\mathcal{L}_2\phi\big(\|\mathbf{x} - \widetilde{\mathbf{x}}_i^{(j)}\|\big)\right\}_{i=1}^{q},$$

and the polynomial basis $\{p_k(\mathbf{x})\}_{k=1}^{l}$. The local RBF–HFD weights are therefore obtained from

$$\begin{pmatrix} \boldsymbol{\Phi} & \boldsymbol{\Psi}_2 & \mathbf{P} \\ \boldsymbol{\Psi}_1 & \boldsymbol{\Psi}_{12} & \mathbf{0} \\ \mathbf{P}^{\mathrm{T}} & \mathbf{0}^{\mathrm{T}} & \mathbf{0} \end{pmatrix} \begin{pmatrix} \mathbf{w}^{(j)} \\ \widetilde{\mathbf{w}}^{(j)} \\ \mathbf{v}^{(j)} \end{pmatrix} = \begin{pmatrix} \left(\mathcal{L}_1\phi\big(\|\mathbf{x}_j - \mathbf{x}_i^{(j)}\|\big)\right)_{i=1}^{m} \\ \left(\mathcal{L}_1\mathcal{L}_2\phi\big(\|\mathbf{x}_j - \widetilde{\mathbf{x}}_i^{(j)}\|\big)\right)_{i=1}^{q} \\ \left(\mathcal{L}p_k(\mathbf{x}_j)\right)_{k=1}^{l} \end{pmatrix}. \quad (40)$$

Here, $\boldsymbol{\Phi}$ and $\mathbf{P}$ have the same roles as in the standard RBF interpolation system, restricted to the current local stencil. The additional blocks arise from the Hermite information. More precisely,

$$(\boldsymbol{\Psi}_2)_{i,j} = \mathcal{L}_2\phi\big(\|\mathbf{x}_i - \widetilde{\mathbf{x}}_j\|\big), i = 1, 2, \ldots, m, \; j = 1, 2, \ldots, q, \quad (41)$$

$$(\boldsymbol{\Psi}_1)_{i,j} = \mathcal{L}_1\phi\big(\|\widetilde{\mathbf{x}}_i - \mathbf{x}_j\|\big), i = 1, 2, \ldots, q, \; j = 1, 2, \ldots, m, \quad (42)$$

and

$$(\boldsymbol{\Psi}_{12})_{i,j} = \mathcal{L}_1\mathcal{L}_2\phi\big(\|\widetilde{\mathbf{x}}_i - \widetilde{\mathbf{x}}_j\|\big), \; i, j = 1, 2, \ldots, q. \quad (43)$$

The vector containing the Hermite weights is

$$\widetilde{\mathbf{w}}^{(j)} = [\widetilde{w}_1^{(j)}, \widetilde{w}_2^{(j)}, \ldots, \widetilde{w}_q^{(j)}]^{\mathrm{T}}.$$

In the expressions above, $\mathcal{L}_1$ and $\mathcal{L}_2$ indicate that the differential operator $\mathcal{L}$ acts on the first and second arguments of the radial kernel, respectively. The mixed block $\boldsymbol{\Psi}_{12}$ consequently contains the action of the operator with respect to both arguments. Under the standard positive-definiteness assumptions on the RBF, the local Hermite system (40) is nonsingular.[32,33] Once this system is solved, only the vectors $\mathbf{w}^{(j)}$ and $\widetilde{\mathbf{w}}^{(j)}$ are needed to construct the discrete differential operator; the auxiliary polynomial coefficient vector $\mathbf{v}^{(j)}$ is not used subsequently.

4. Numerical examples

This section presents three test problems to study the performance and accuracy of the RBF-HFD method. To measure the temporal convergence, the experimental convergence rate $C_{\delta t}$ is calculated by

$$C_{\delta t} = \log_2\left(\frac{\|L^{\infty}(2\delta t, h)\|}{\|L^{\infty}(\delta t, h)\|}\right).$$

The maximum error at the final time T is defined as $L^{\infty} = \max_{1 \le j \le N-1} |U(\mathbf{x}_j, T) - u(\mathbf{x}_j, T)|$. During the numerical simulations, we use the polyharmonic spline (PHS) RBF $\phi(r) = r^5$, where $r = \|\mathbf{x} - \mathbf{x}_j\|_2$ is the Euclidean distance between the evaluation point $\mathbf{x}$ and the jth RBF center. All numerical experiments were performed in MATLAB R2023b on a personal computer equipped with an Intel(R) Core(TM) i5-8500 processor running at 3.00 GHz with 16 GB of RAM.

Example 1. We consider the two-dimensional TFCDR-OCP (1) on the unit square $\Omega = [0, 1]^2$. The model parameters are chosen as $\boldsymbol{\nu} = (1, 0)$, $w = 1$, and $\lambda = 10^{-6}$. For this test problem, the initial data y_0 and the desired state y_d are determined through the optimality system by prescribing the analytic state and control functions,

respectively, as follows:

$$\bar{y}(x_1, x_2, t) = \exp(-t)\sin(2\pi x_1)\sin(2\pi x_2),$$

and

$$\bar{u}(x_1, x_2, t) = \exp(-t)(1-t)\sin(2\pi x_1)\sin(2\pi x_2).$$

Table 1 lists the temporal convergence of the localized RBF-HFD method in the L_∞ norm for the state and adjoint variables with $N = 289$, $m = 17$ and $q = 3$. The results confirm the second-order temporal accuracy of the localized RBF-HFD method for both the state and adjoint variables as N_t increases. **Table 2** indicates that the proposed method achieves competitive accuracy for the state variable and considerably smaller errors for the adjoint variable than the CIRBF method. **Table 3** highlights the improved accuracy obtained with larger stencil sizes while maintaining moderate condition numbers and CPU times. These results demonstrate the accuracy and efficiency of the localized RBF-HFD formulation. **Figure 1** presents the sparsity patterns of the local matrices for different stencil sizes. **Figures 2** and **3** illustrate the good agreement between the approximate and analytical solutions of the adjoint and state variables, respectively, at selected time levels. Finally, **Figure 4** shows the numerical control solutions and their corresponding absolute errors at $t = 0.2$ and $t = 0.5$ with $N = 289$, $N_t = 50$ and $m = 17$.

Example 2. We consider the one-dimensional TFCDR-OCP (1) on $\Omega = [0, 1]$, with $w = 0$, $\nu = 0$, $\lambda = 10^{-6}$, and

$$\begin{aligned} y_d = {} & t^2(1-t)^3x(x-1) \\ & + \nu\Big(12t(t-1)^2x(x-1) + 2(t-1)^3x(x-1) \\ & - 4t(t-1)^3 - 6t^2(t-1)^2 \\ & + 3t^2\Big(6t^2(t-1)^2 + 4t(t-1)^3 \\ & + 2t - 20x(x-1)\Big)\Big). \end{aligned}$$

The analytical solutions for this example can be expressed in the following form:

$$\bar{y} = x(x-1)t^2(1-t)^3,$$

and

$$\bar{p} = \nu\Big(3t^2(t-1)^2x(x-1) + 2t(t-1)^3x(x-1) - 2t^2(t-1)^3\Big).$$

Table 1. Temporal convergence of the RBF-HFD method in the L_∞ norm for the state and adjoint variables in Example 1

N_t	$L_\infty(y)$	$C_{\delta t}$	$L_\infty(p)$	$C_{\delta t}$
10	7.3066E−06	—	2.2915E−11	—
20	1.6239E−06	2.1697	5.5166E−12	2.0545
40	4.0600E−07	1.9999	1.3795E−12	1.9996
80	1.0151E−07	1.9999	3.4490E−13	1.9999
160	2.5377E−08	2.0000	8.6226E−14	2.0000
320	6.3442E−09	2.0000	2.1557E−14	2.0000
640	1.5860E−09	2.0000	5.3892E−15	2.0000
1280	3.9651E−10	2.0000	1.3473E−15	2.0000

Table 2. Comparison of the L_∞ errors obtained by the RBF-HFD and CIRBF methods for the adjoint and state functions in Example 1

t	$\|y - \bar{y}\|_{L_\infty}$		$\|p - \bar{p}\|_{L_\infty}$	
	RBF-HFD	**CIRBF[27]**	**RBF-HFD**	**CIRBF[27]**
0.2	$8.7310E-06$	$7.1370E-06$	$4.4580E-08$	$6.9320E-04$
0.5	$4.2190E-06$	$5.3300E-06$	$3.3030E-08$	$5.1390E-04$
0.8	$1.4590E-06$	$3.9480E-06$	$2.4460E-08$	$3.8100E-04$

Table 3. Computational efficiency and accuracy of the RBF-HFD method for different spatial node numbers and stencil sizes in Example 1

N	m	$L_\infty(y)$	$L_\infty(p)$	condest(K)	CPU (s)
14	11	2.2607E−02	4.8459E−05	3.3193E+02	0.9172
14	15	3.2010E−04	7.0626E−07	1.8231E+02	0.7481
14	19	1.0724E−04	2.3855E−07	1.7910E+02	0.6866
19	11	3.4547E−02	1.5025E−04	2.3540E+03	1.5780
19	15	1.2642E−04	2.0591E−07	2.8121E+02	1.5842
19	19	6.4942E−05	1.2760E−07	3.0684E+02	1.6929
21	11	9.0928E−03	6.5229E−06	4.2013E+02	2.4058
21	15	1.0681E−04	1.4829E−07	3.5651E+02	2.1558
21	19	6.1979E−05	1.0620E−07	3.8560E+02	2.3953

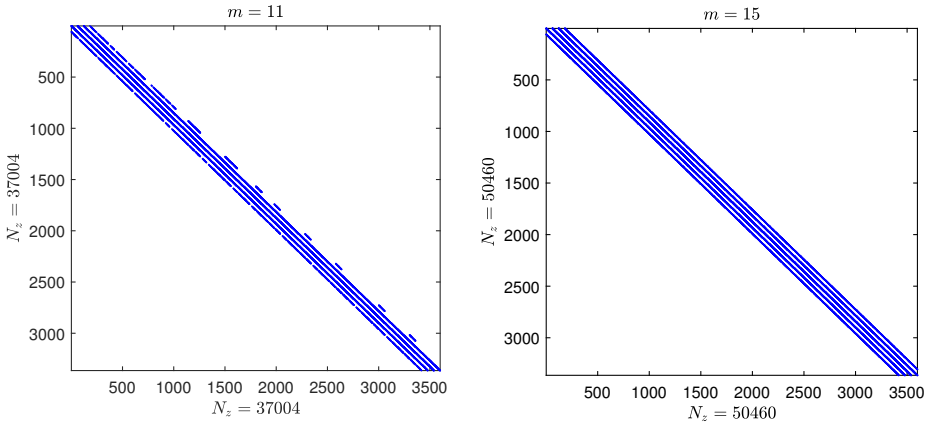


Figure 1. Sparsity structures of the relevant matrix for different stencil sizes, $m = 11$ and $m = 15$

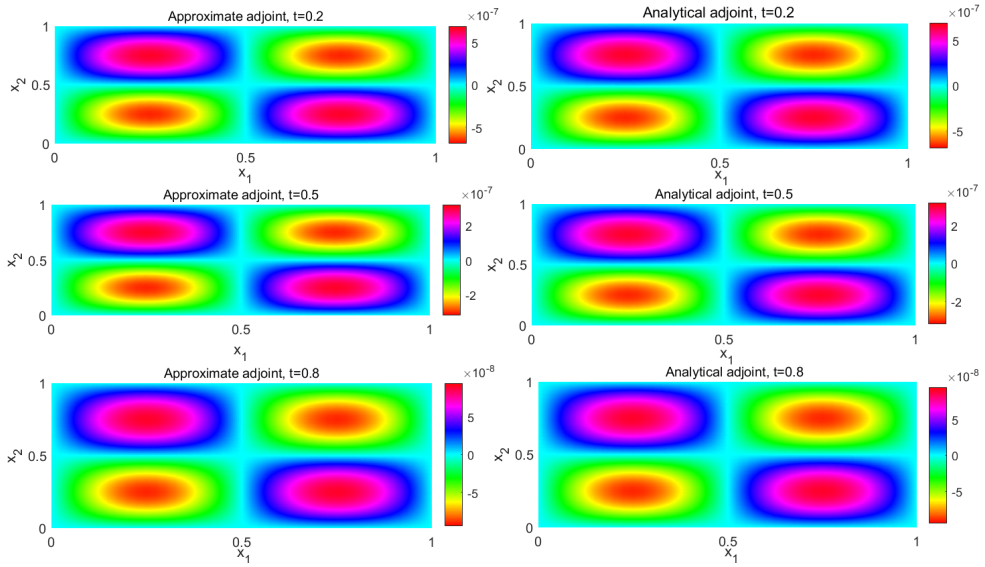


Figure 2. Comparison of the approximate and analytical solutions of the adjoint variable p at $t = 0.2$, 0.5, and 0.8 in Example 1

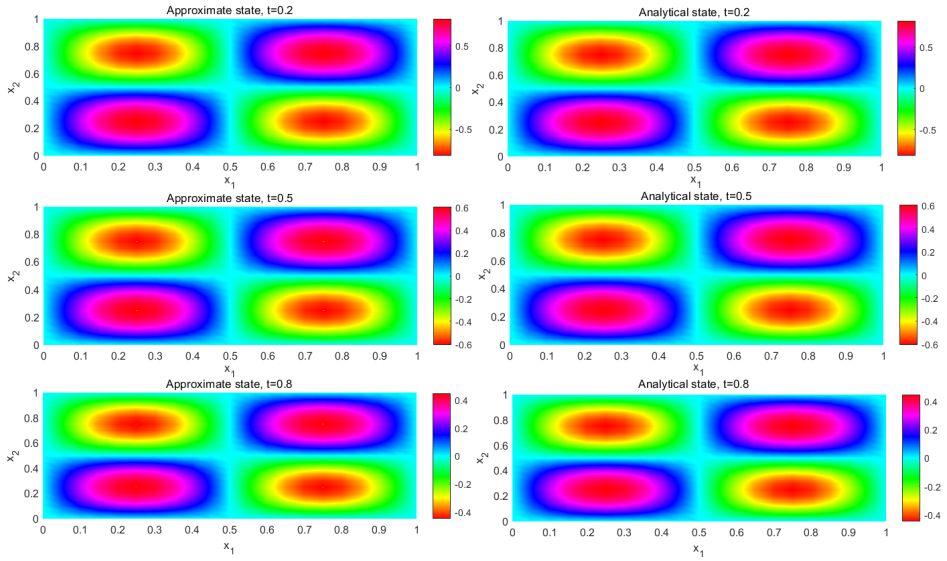


Figure 3. Comparison of the approximate and analytical solutions of the state variable y at $t = 0.2$, 0.5, and 0.8 in Example 1

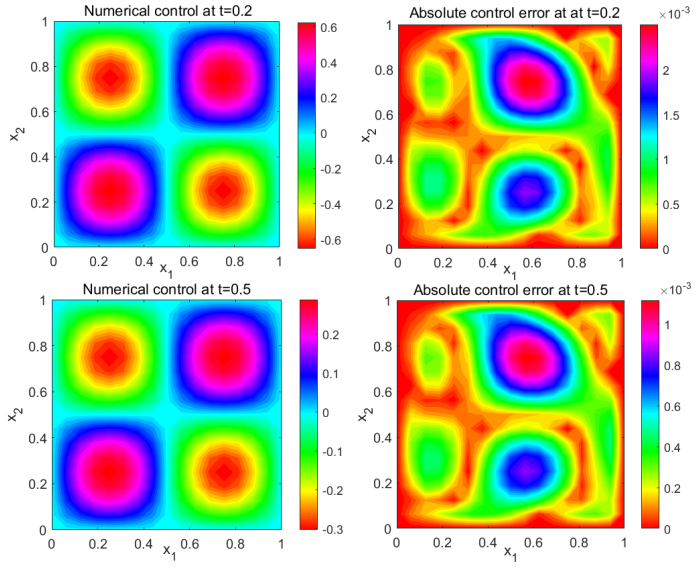


Figure 4. Numerical solutions of the optimal control and the corresponding absolute errors at $t = 0.2$ and $t = 0.5$ in Example 1

Table 4 presents the temporal convergence results in terms of the L_∞ and RMS errors for the state variable y at $t = 0.5$ with $N = 41$, $m = 7$, and $q = 2$. The results indicate that both errors decrease consistently as N_t increases, with the observed convergence rates approaching second order. **Table 5** reveals that the RBF-HFD method produces smaller L_∞ errors than the CIRBF and barycentric approaches at all reported time levels. **Table 6** highlights the smaller RBF-HFD errors for the adjoint variable and the L_2 norm of the state, whereas the L_∞ state error varies over time. **Table 7** shows the high accuracy of the RBF-HFD method across all tested node numbers and stencil sizes. The low CPU times and moderate condition numbers also indicate its computational efficiency and robustness. **Figure 5** illustrates the space–time distributions of the absolute errors in the state and adjoint variables. **Figure 6** presents the exact and approximate solutions at selected time levels, demonstrating good agreement between them. Finally, **Figure 7** examines the influence of the fractional order β on the state and adjoint solutions.

Table 4. Temporal error behavior of the state variable y at $t = 0.5$ for Example 2

N_t	L_∞	$C_{\delta t}^{L_\infty}$	RMS	$C_{\delta t}^{\mathrm{RMS}}$	CPU (s)
10	3.2606E−08	—	2.3733E−08	—	0.005
20	2.0665E−10	7.3018	1.6130E−10	7.2010	0.014
40	3.5449E−11	2.5434	2.7461E−11	2.5543	0.036
80	8.1112E−12	2.1277	6.1878E−12	2.1499	0.168
160	1.9338E−12	2.0685	1.4625E−12	2.0810	0.899

Table 5. Comparison of the L_∞ errors of the state function obtained by the RBF-HFD, CIRBF, and barycentric methods in Example 2

t	$\|y - \bar{y}\|_{L_\infty}$		
	RBF-HFD	CIRBF[27]	RBC[26]
0.2	2.5694E−10	6.5900E−08	6.1350E−07
0.5	3.5449E−11	3.0690E−08	4.1300E−07
0.7	1.3157E−10	4.2460E−08	2.9920E−07
0.9	6.9651E−09	2.4400E−08	1.6240E−07

Table 6. Comparison of the L_∞ and L_2 errors of the adjoint and state functions computed by the CIRBF and RBF-HFD methods for Example 2

t	$L_2(y)$		$L_2(p)$		$L_\infty(y)$		$L_\infty(p)$	
	CIRBF^{27}	**RBF-HFD**	**CIRBF^{27}**	**RBF-HFD**	**CIRBF^{27}**	**RBF-HFD**	**CIRBF^{27}**	**RBF-HFD**
0.2	1.39E−04	6.85E−09	2.10E−04	4.56E−10	6.59E−08	7.87E−09	8.16E−08	6.25E−10
0.5	2.08E−04	2.31E−08	3.21E−04	2.24E−11	3.07E−08	3.26E−08	1.57E−07	3.07E−11
0.7	8.89E−05	2.15E−07	1.36E−04	1.64E−10	4.25E−08	3.03E−07	9.07E−08	2.24E−10
0.9	4.00E−06	1.92E−06	8.20E−06	6.31E−11	2.44E−08	2.71E−06	3.09E−08	8.64E−11

Table 7. Computational efficiency and accuracy of the RBF-HFD method for different spatial node numbers and stencil sizes in Example 2

N	m	$L_\infty(y)$	$L_\infty(p)$	$L_\infty(u)$	condest(K)	CPU (s)
11	5	2.0656E−10	4.6174E−12	4.6174E−06	2.3132E+02	0.0822
11	7	2.0689E−10	4.6174E−12	4.6174E−06	2.6615E+02	0.0292
11	9	2.0669E−10	4.6175E−12	4.6175E−06	2.6938E+02	0.0253
21	5	2.0664E−10	4.6174E−12	4.6174E−06	5.1765E+02	0.0639
21	7	2.0673E−10	4.6174E−12	4.6174E−06	6.1789E+02	0.1014
21	9	2.0666E−10	4.6174E−12	4.6174E−06	6.6372E+02	0.0559
31	5	2.0666E−10	4.6174E−12	4.6174E−06	9.9302E+02	0.1409
31	7	2.0671E−10	4.6174E−12	4.6174E−06	1.2175E+03	0.1648
31	9	2.0667E−10	4.6174E−12	4.6174E−06	1.3217E+03	0.1742
41	5	2.0667E−10	4.6174E−12	4.6174E−06	1.6583E+03	0.3044
41	7	2.0670E−10	4.6174E−12	4.6174E−06	2.0571E+03	0.2708
41	9	2.0668E−10	4.6174E−12	4.6174E−06	2.2429E+03	0.2711

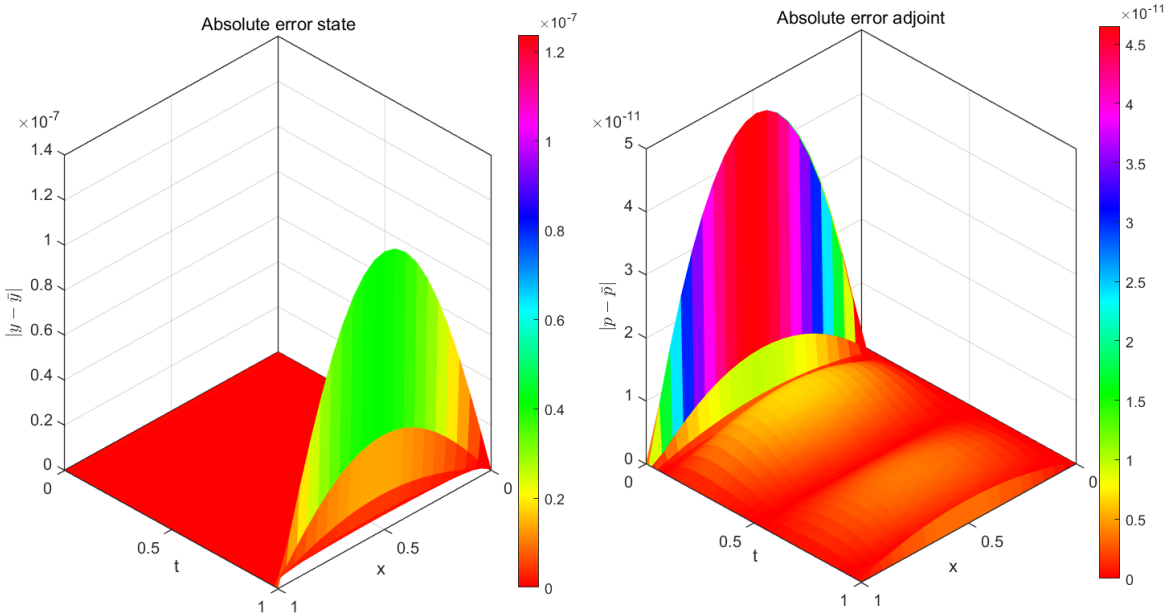


Figure 5. Space–time distributions of the absolute errors associated with the state variable y (left) and the adjoint variable p (right) in Example 2

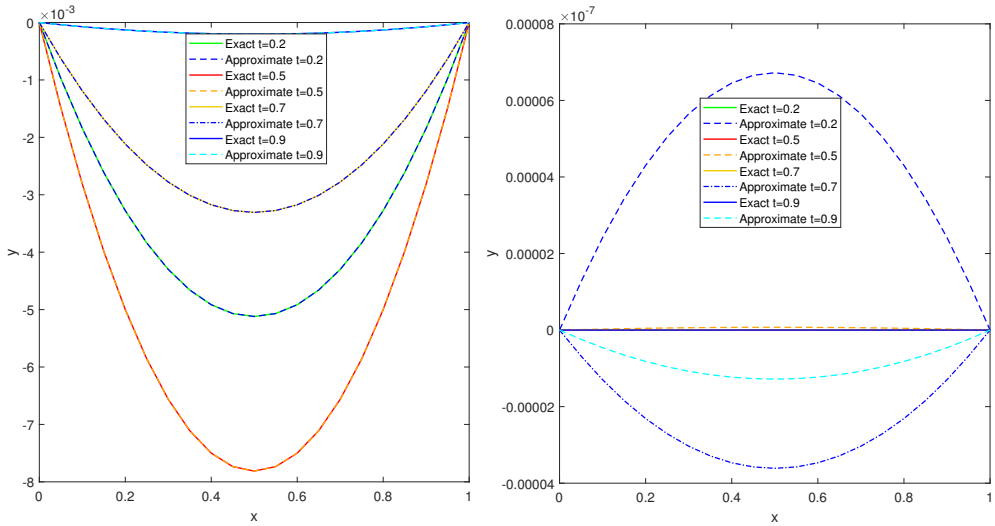


Figure 6. Comparison of the exact and approximate solutions of the state variable y (left) and the adjoint variable p (right) at $t \in \{0.2, 0.5, 0.7, 0.9\}$ in Example 2

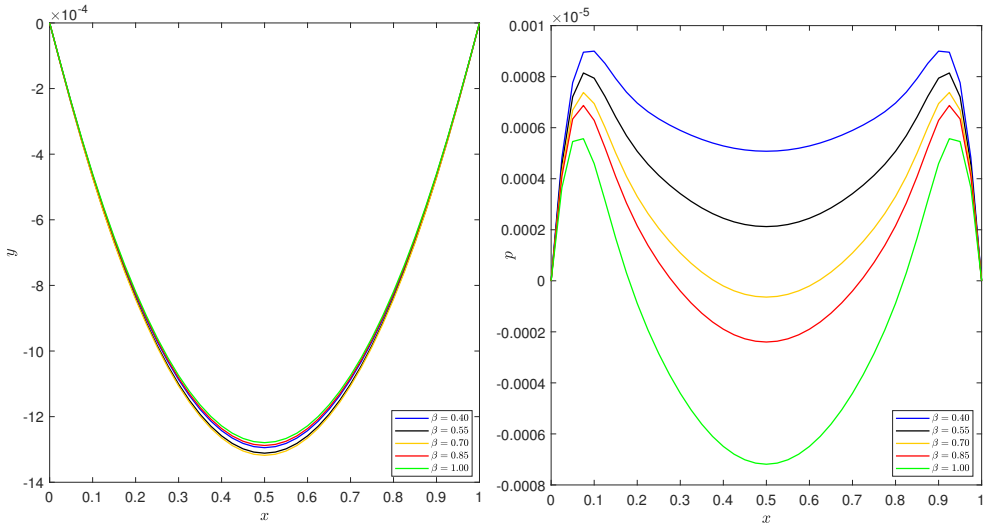


Figure 7. Behavior of the approximate solutions of the state variable y (left) and the adjoint variable p (right) for $\beta \in \{0.40, 0.55, 0.70, 0.85, 1.00\}$ in Example 2

Example 3. We consider the three-dimensional TFCDR-OCP (1) on the unit cube $\Omega = [0,1]^3$. The model parameters are chosen as $\boldsymbol{\nu} = (1,1,1)$, $w = 0$, $\lambda = 10^{-6}$, and $\beta = 0.5$. For this test problem, the desired state y_d is determined through the optimality system by prescribing the analytic state and control functions, respectively, as follows:

$$\bar{y}(x,y,z,t) = t^3(1-t)^3 \sin(2\pi x)\sin(2\pi y)\sin(2\pi z),$$

and

$$\bar{u}(x,y,z,t) = -t^3(1-t)^3 \sin(2\pi x)\sin(2\pi y)\sin(2\pi z).$$

Table 8 reports the L_∞ errors of the state, adjoint, and control variables at selected time levels. The results indicate high accuracy for the state and adjoint approximations. **Figure 8** illustrates the approximate adjoint solution and its absolute error at $t = 0.5$ with $N = 343$ and $m = 35$. The results demonstrate good agreement between the numerical and analytical solutions. Finally, **Figure 9** presents the approximate state solution and its absolute error at $t = 0.5$. The small errors indicate the accuracy of the proposed method.

Table 8. Absolute errors of the state y, adjoint p, and control u variables at selected time levels in Example 3

t	$L_\infty(y)$	$L_\infty(p)$	$L_\infty(u)$
0.2	2.1164E−07	1.6117E−09	1.6117E−03
0.5	8.3156E−07	6.3731E−09	6.3731E−03
0.8	9.0831E−07	1.3315E−09	1.3315E−03

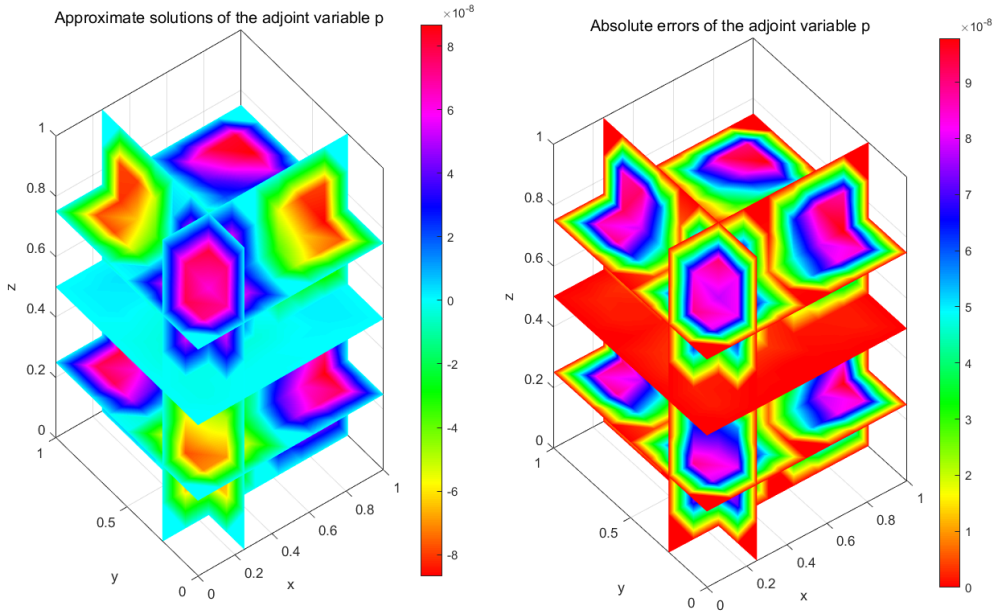


Figure 8. Approximate solutions and absolute errors of the adjoint variable p at $t = 0.5$ with $N_t = 10$ in Example 3

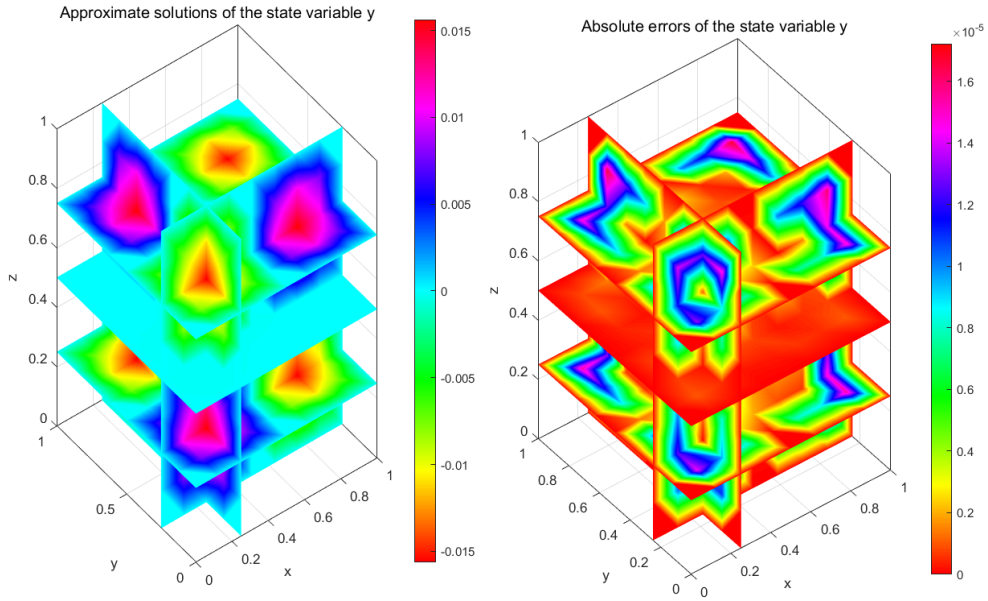


Figure 9. Approximate solutions and absolute errors of the state variable y at $t = 0.5$ with $N_t = 10$ in Example 3

5. Conclusion

This paper applied a localized meshless strategy for the numerical solution of TFCDR-OCPs. The time-fractional derivative was discretized by a shifted Grünwald-type approximation, while the spatial operators involved in the state and adjoint equations were treated using the RBF-HFD method. The use of local Hermite RBF approximations allowed the spatial discretization to be constructed on small overlapping neighborhoods. As a result, the need for large global interpolation systems was avoided, while the meshless character of the method was retained. The stability and convergence properties of the resulting numerical formulation were also investigated theoretically. The proposed method was assessed through three numerical examples. The results showed that the RBF-HFD formulation yielded accurate approximations for both the state and adjoint variables.

Its combination with the shifted Grünwald discretization in time also led to an efficient treatment of the fractional optimal control problem. The overall findings indicated that the method can be applied to more complex fractional control models and higher-dimensional settings in future work.

Acknowledgements

None.

Funding

None.

Conflict of interest

The author declares that there are no conflicts of interest.

Author contributions

This is a single-authored article.

Availability of data

No datasets were analysed or generated during the current paper.

AI tools statement

The author confirms that no AI tools were used in the preparation of this manuscript.

References

1. Wu H, He L, Hu Y, He J. Discrete stochastic optimal control for multi-stakeholder governance of crop rotation and fallow insurance. *Int J Optim Control Theor Appl.* 2026;16(5):026330208. https://doi.org/10.36922/IJOCTA026330208
2. Kien BT, Fedorov VE, Phuong TD. Optimal control problems governed by fractional differential equations with control constraints. *SIAM J Control Optim.* 2022;60(3):1732–1762. https://doi.org/10.1137/21M1430728
3. Malmir I. New pure multi-order fractional optimal control problems with constraints: QP and LP methods. *ISA Trans.* 2024;153:155–190. https://doi.org/10.1016/j.isatra.2024.08.003
4. Taifi K, Sabbar Y, Özdemir N. Impact of socioeconomic and healthcare structure on epidemic dynamics: mathematical modeling and optimal control. *Int J Optim Control Theor Appl.* 2026;16(5):026240117. https://doi.org/10.36922/IJOCTA026240117
5. Zhu J, Zeng QC. A mathematical formulation for optimal control of air pollution. *Sci China Ser D Earth Sci.* 2003;46:994–1002. https://doi.org/10.1007/BF02959394
6. Chugh S, Dhar J, Guha RK. An innovation diffusion model with two innovations under two simultaneous effects in a competitive market: coexistence through optimal control. *J Math Comput Sci.* 2024;35(1):1–15. https://doi.org/10.22436/jmcs.035.01.01
7. Martínez A, Rodríguez C, Vázquez-Méndez ME. Theoretical and numerical analysis of an optimal control problem related to wastewater treatment. *SIAM J Control Optim.* 2000;38(5):1534–1553. https://doi.org/10.1137/S0363012998345640
8. Darehmiraki M, Farahi MH, Effati S. A novel method to solve a class of distributed optimal control problems using Bezier curves. *J Comput Nonlinear Dyn.* 2016;11(6):061008. https://doi.org/10.1115/1.4033755
9. Gunzburger MD. *Perspectives in Flow Control and Optimization.* Philadelphia, PA: Society for Industrial and Applied Mathematics; 2003. https://doi.org/10.1137/1.9780898718720
10. Herzog R, Kunisch K. Algorithms for PDE-constrained optimization. *GAMM-Mitt.* 2010;33(2):163–176. https://doi.org/10.1002/gamm.201010013
11. Hinze M, Rösch A. Discretization of optimal control problems. In: *Constrained Optimization and Optimal Control for Partial Differential Equations.* Basel, Switzerland: Springer; 2012:391–430. https://doi.org/10.1007/978-3-0348-0133-1_21
12. LeVeque RJ. *Finite Difference Methods for Ordinary and Partial Differential Equations: Steady-State and Time-Dependent Problems.* Philadelphia, PA: Society for Industrial and Applied Mathematics; 2007. https://doi.org/10.1137/1.9780898717839
13. Johnson C. *Numerical Solution of Partial Differential Equations by the Finite Element Method.* Chelmsford, MA: Courier Corporation; 2012.
14. Borzì A, Schulz V. Multigrid methods for PDE optimization. *SIAM Rev.* 2009;51(2):361–395. https://doi.org/10.1137/060671590
15. Briggs WL, Henson VE, McCormick SF. *A Multigrid Tutorial.* 2nd ed. Philadelphia, PA: Society for Industrial and Applied Mathematics; 2000. https://doi.org/10.1137/1.9780898719505
16. Nocedal J, Wright SJ. *Numerical Optimization.* 2nd ed. New York, NY: Springer; 2006. https://doi.org/10.1007/978-0-387-40065-5
17. Antoniou A, Lu WS. *Practical Optimization: Algorithms and Engineering Applications.* 2nd ed. New York, NY: Springer; 2021. https://doi.org/10.1007/978-1-0716-0843-2
18. Tajadodi H, Jafari H, Ncube MN. Genocchi polynomials as a tool for solving a class of fractional optimal control problems. *Int J Optim Control Theor Appl.* 2022;12(2):160–168. https://doi.org/10.11121/ijocta.2022.1263

19. Baleanu D, Hajipour M, Jajarmi A. An accurate finite difference formula for the numerical solution of delay-dependent fractional optimal control problems. *Int J Optim Control Theor Appl.* 2024;14(3):183–192. https://doi.org/10.11121/ijocta.1478
20. Youssri YH, Abd-Elhameed WM. Spectral tau algorithm for solving a class of fractional optimal control problems via Jacobi polynomials. *Int J Optim Control Theor Appl.* 2018;8(2):152–160. https://doi.org/10.11121/ijocta.01.2018.00442
21. Hassani H, Tenreiro Machado JA, Naraghirad E. Generalized shifted Chebyshev polynomials for fractional optimal control problems. *Commun Nonlinear Sci Numer Simul.* 2019;75:50–61. https://doi.org/10.1016/j.cnsns.2019.03.013
22. Hassani H, Avazzadeh Z, Tenreiro Machado JA, Naraghirad E. A new hybrid method for two dimensional nonlinear variable order fractional optimal control problems. *Asian J Control.* 2021;23(4):2004–2018. https://doi.org/10.1002/asjc.2351
23. Hassani H, Tenreiro Machado JA, Hosseini Asl MK, Dahaghin MS. Numerical solution of nonlinear fractional optimal control problems using generalized Bernoulli polynomials. *Optim Control Appl Methods.* 2021;42(4):1045–1063. https://doi.org/10.1002/oca.2715
24. Lions JL. *Optimal Control of Systems Governed by Partial Differential Equations.* Berlin, Germany: Springer; 1971. https://doi.org/10.1007/978-3-642-65024-6
25. Tröltzsch F. *Optimal Control of Partial Differential Equations: Theory, Methods, and Applications.* Providence, RI: American Mathematical Society; 2010. https://doi.org/10.1090/gsm/112
26. Darehmiraki M, Rezazadeh A. A new solution for optimal control of fractional convection–reaction–diffusion equation using rational barycentric interpolation. *Bull Iran Math Soc.* 2020;46(5):1307–1340. https://doi.org/10.1007/s41980-019-00327-y
27. Mahmoudi M, Shojaeizadeh T, Darehmiraki M. Optimal control of time-fractional convection–diffusion–reaction problem employing compact integrated RBF method. *Math Sci.* 2023;17(1):1–14. https://doi.org/10.1007/s40096-021-00434-0
28. Fasshauer GE. *Meshfree Approximation Methods with MATLAB.* Singapore: World Scientific; 2007. https://doi.org/10.1142/6437
29. Wendland H. *Scattered Data Approximation.* Cambridge, UK: Cambridge University Press; 2004. https://doi.org/10.1017/CBO9780511617539
30. Nikan O. A localized meshless collocation technique for the distributed-order time-fractional modified anomalous subdiffusion equation. *Int Commun Heat Mass Transfer.* 2026;180:112655. https://doi.org/10.1016/j.icheatmasstransfer.2026.112655
31. Nikan O, Avazzadeh Z. Numerical simulation of the time-fractional nonlinear Schrödinger equation and the time-fractional Schrödinger–Poisson system. *Mathematics.* 2026;14(20):3731. https://doi.org/10.3390/math14203731
32. Wu ZM. Hermite–Birkhoff interpolation of scattered data by radial basis functions. *Approx Theory Appl.* 1992;8(2):1–10. https://doi.org/10.1007/BF02836101
33. Narcowich FJ, Ward JD. Generalized Hermite interpolation via matrix-valued conditionally positive definite functions. *Math Comp.* 1994;63(208):661–687. https://doi.org/10.1090/S0025-5718-1994-1254147-6

Omid Nikan *is an Assistant Professor in the School of Mathematics and Computer Science at Iran University of Science and Technology (IUST), Tehran, Iran. He received his Ph.D. in Applied Mathematics from IUST in 2020. His research interests include numerical analysis, partial differential equations, fractional differential equations, meshless methods, and computational mathematics. He has been listed among the top 1% of scientists worldwide since 2024.*
https://orcid.org/0000-0003-3041-8726

This work is licensed under a Creative Commons Attribution 4.0 International License. The authors retain ownership of the copyright for their article, but they allow anyone to download, reuse, reprint, modify, distribute, and/or copy articles in IJOCTA, so long as the original authors and source are credited. To see the complete license contents, please visit http://creativecommons.org/licenses/by/4.0/.